Porosity Evolution in Rate and State Friction

John W. Rudnicki[1]

[1]Northwestern University

November 23, 2022

Abstract

This letter compares the predictions of the two expressions that have been proposed for the porosity evolution in the context of rate and state friction. One depends only on the sliding velocity; the other depends only on the state variable. The predictions of the two expressions are similar for simulations of velocity stepping and slide-hold-slide experiments but differ significantly for normal effective stress jumps at constant sliding velocity. The formulation that depends only on the velocity predicts no change in the porosity; the other does.

A simulation with a spring-block model indicates that the magnitude of rapid slip events is essentially the same for the two models. Variations of porosity and induced pore pressure near rapid slip events are similar and consistent with experimental observations. Predicted porosity variations during slow slip intervals and the time at which rapid slip events occur are significantly different.

Porosity Evolution in Rate and State Friction

John W. Rudnicki

[1]Department of Civil and Environmental Engineering and Department of Mechanical Engineering, Northwestern University, Evanston, IL 60208-3109

Key Points:

- Two formulations that have been suggested for porosity evolution give similar results for simulated velocity stepping and slide-hold- tests.
- The two formulations give significantly different results for effective normal stress changes at constant slip velocity.
- A spring - block simulation indicates that both formulations predict pore pressure change near rapid slip events consistent with laboratory observations.

Corresponding author: John W. Rudnicki, jwrudn@northwestern.edu

Abstract

This letter compares the predictions of the two expressions that have been proposed for the porosity evolution in the context of rate and state friction. One depends only on the sliding velocity; the other depends only on the state variable. The predictions of the two expressions are similar for simulations of velocity stepping and slide-hold-slide experiments but differ significantly for normal effective stress jumps at constant sliding velocity. The formulation that depends only on the velocity predicts no change in the porosity; the other does. A simulation with a spring-block model indicates that the magnitude of rapid slip events is essentially the same for the two models. Variations of porosity and induced pore pressure near rapid slip events are similar and consistent with experimental observations. Predicted porosity variations during slow slip intervals and the time at which rapid slip events occur are significantly different.

Plain Language Summary

The interaction of pore fluid and deformation is important for many geological processes and for technological applications involving fluid injection, such as carbon sequestration, disposal of waste fluids from hydraulic fracturing, and geothermal stimulation. Often these applications have induced earthquakes that have raised cause for concern. An important element of the interaction of pore fluid and deformation is the evolution of porosity, that is, the ratio of volume of voids to the total volume, with the slip on a fault surface. If the porosity increases more rapidly that pore fluid can diffuse out of pores, the pore pressure decreases and increases the frictional resistance to slip; conversely, porosity decreases can increase the pore pressure and reduce the frictional resistance to slip. This paper compares two proposed descriptions for porosity evolution with slip. Both have similar predictions for standard laboratory experiments but differ significantly for changes of pore fluid pressure at constant sliding velocity. In simulations with a simple spring - block model both predict changes in pore fluid pressure with time near rapid slip events that are consistent with experiments. The predicted changes in porosity differ in the intervals of slow slip between rapid slip events.

Introduction

The interaction of pore fluid with mechanical deformation affects many geological processes and technological applications involving the injection or withdrawal of fluid. Cases in which the applications have induced seismicity have raised concerns about whether they should be continued. Seismic activity has been induced by injection for the disposal of wastes (Healy et al., 1968; Raleigh et al., 1976; Hsieh & Bredehoeft, 1981; Zoback & Harjes, 1997; Ake et al., 2005; Kim, 2013), including water from hydraulic fracturing (Horton, 2012; Ellsworth, 2013; Keranen et al., 2013, 2014; Weingarten et al., 2015; Barbour et al., 2017), geothermal stimulation (Majer et al., 2007; Charéty et al., 2007; Deichmann & Giardini, 2009; Martinez-Garzón et al., 2014; Lengliné et al., 2017), and CO_2 sequestration (Evans et al., 2012) and by withdrawal for gas production (Segall et al., 1994).

A key element in the interaction of pore fluid with deformation is the evolution of porosity (Segall & Rice, 1995; Segall et al., 2010; Yang & Dunham, 2021; Heimisson et al., 2021). This paper examines and compares two proposals for this evolution (Segall & Rice, 1995; Sleep, 1995) in the context of rate and state friction. In this theory, the coefficient of friction depends on the rate of slip and on a state variable that characterizes the evolving nature of the slip surface. A large number of experiments (Marone, 1998) has established that this formulation provides a robust description of slip on rock surfaces or gouge layers, at least at low sliding velocities. When this description is used in models of faulting, it exhibits a rich spectrum of behavior, including slip velocity of various magnitudes and episodes of rapid slip alternating with restrengthening at low velocities, and has been an important contribution to better understanding the mechanics of earthquakes (e.g, Lapusta et al., 2000; Liu & Rice, 2005; Ampuero & Rubin, 2008; Lapusta & Barbot, 2012).

One expression for the porosity evolution was proposed by Segall and Rice (1995) (hereafter abbreviated SR) based on experiments by Marone et al. (1990) on quartz gouge. This expression depends on the sliding velocity, but not on the state. SR also discuss a second formulation which they attribute to Sleep (1995) (hereafter abbreviated SL). This form depends on the state, but not on the slip velocity. Both forms also depend on a parameter ε that scales the magnitude of the porosity change. Several experiments (Linker & Dieterich, 1992; Hong & Marone, 2005) have observed that changes in effective normal stress at constant slip velocity cause changes in state. Because changes in pore pressure change the effective normal stress, the difference between the total normal stress and the pore fluid pressure, the porosity for the SL form will change but not for the SR form. This difference can be important in processes involving the interaction of deformation with pore fluid diffusion.

Rate and State Friction

The expression for the shear stress for rate and state friction is (Dieterich, 1979, 1980; Ruina, 1983)

$$\tau = \bar{\sigma}\left\{\mu_0 + a\ln\left(v/v_0\right) + b\ln\left(\theta/\theta_0\right)\right\} \tag{1}$$

where τ is the friction stress, $\bar{\sigma}$ is the effective normal stress, that is, the difference between the total compressive normal stress σ and the pore fluid pressure p, v is the sliding velocity, and θ is a state variable that reflects the evolution of the sliding surface. v_0 and θ_0 are arbitrary reference values. μ_0 is the friction coefficient for steady slip at the reference values, typically around 0.6 (Byerlee, 1978). Although θ has been interpreted as the age of asperity contacts, recent experiments (Bhattacharya et al., 2022) have called into question this interpretation.

The empirical parameters a and b are typically small, of order 0.01, but they control the stability of slip. Evolution of the state variable is generally described by one of two equations: the aging law

$$\frac{d\theta}{dt} = 1 - \frac{\theta v}{d_c} \tag{2}$$

or the slip law

$$\frac{d\theta}{dt} = -\frac{v\theta}{d_c}\ln\left(\frac{v\theta}{d_c}\right) \tag{3}$$

where d_c is the decay length of the exponential decay of θ following a sudden change in velocity. The principal difference between (2) and (3) is their behavior for zero velocity. In this case, the state increases linearly in time for the aging law but does not change for the slip law. For slip at a steady state value v_{ss}, $d\theta/dt = 0$ and $\theta = d_c/v_{ss}$. Substitution into (1) gives

$$\tau_{ss} = \bar{\sigma}\left\{\mu_0 + (a-b)\ln\left(v_{ss}/v_0\right)\right\} \tag{4}$$

For $a > b$, τ_{ss} increases with v_{ss} and the response is said to be velocity strengthening; for $a < b$, τ_{ss} decreases with v_{ss} and the response is said to be velocity weakening.

Based on their experiments, Linker and Dieterich (1992) proposed that changes of the state caused by changes in effective normal stress could described by subtracting the following term from (2) and (3):

$$\frac{\alpha}{b}\frac{\theta}{\bar{\sigma}}\frac{d\bar{\sigma}}{dt} \tag{5}$$

where α is another parameter that satisfies $0 < \alpha \le \mu_0$ (Linker & Dieterich, 1992; Perfettini et al., 2001; Hong & Marone, 2005).

Based on experiments by Marone et al. (1990) on the shearing of gouge layers of quartz sand at an effective confining stress of 150 MPa, Segall and Rice (1995) proposed the following expression for the rate of change of porosity ϕ:

$$\frac{d\phi}{dt} = -\frac{v}{d_c}\left(\phi - \phi_{ss}\right) \tag{6}$$

where ϕ_{ss} is the steady state value of the porosity. They take ϕ_{ss} to be given by

$$\phi_{ss} = \phi_0 + \varepsilon \ln\left(v/v_0\right) \tag{7}$$

where ϕ_0 is the initial value of porosity and ε reflects the magnitude of the porosity change. Substituting (7) into (6) yields

$$\frac{d\Phi}{dT} = -V\left(\Phi - \varepsilon \ln V\right) \tag{8}$$

where $\Phi = \phi - \phi_0$, $V = v/v_0$, and $T = v_0 t/d_c$ is a nondimensional time. For $v_0 = 10$ μm/s and $d_c = 0.2$ mm, values representative of laboratory experiments, $T = 1$ corresponds to 20 s. For $v_0 = 0.03$ m/year and $d_c = 0.1$ m, values representative of the crust, $T = 1$ corresponds to 4 months.

SR also discuss another expression for the variation in porosity that they attribute to SL. It is given by

$$\Phi = -\varepsilon \ln \Theta \tag{9}$$

where Φ is the change in porosity and $\Theta = \theta v_0/d_c$. SR noted that (8) and (9) are identical for steady state and when linearized about steady state. In addition, if the slip law for the variation of the state (3) is used, then (8) and (9) are identical. (Differentiate (9), use (3), and then use (9) again.)

SR infer $\varepsilon = 1.7 \times 10^{-4}$ from the data of Marone et al. (1990) but use a larger value 1.7×10^{-3} for their simulations of seismic cycles. Samuelson et al. (2009) measured porosity changes on a simulated fine-grained quartz fault under a range of conditions and used the slip law (3) to infer results for ε. They found values ranging from 4.7×10^{-5} to 3.0×10^{-4}. Although it might be expected that ε varies with effective normal stress, Samuelson et al. (2009) found that it did not. Consequently, ε is taken as constant here.

Velocity Stepping at Constant Normal Stress

For a velocity step from V_1 to V_2 at time T_2, the solution of (8), in nondimensional variables, is

$$\Phi\left(T\right) = \varepsilon \ln V_2 - \varepsilon \ln\left(V_2/V_1\right) \exp\left(-V_2\left(T - T_2\right)\right) \tag{10}$$

To determine the porosity change from (9), it is first necessary to determine the variation of the state. For the aging law, the solution is

$$\Theta(T) = \left(\Theta_1 - 1/V_2\right) \exp\left(-V_2\left(T - T_2\right)\right) + 1/V_2 \tag{11}$$

where Θ_1 is the value of Θ at the end of the preceding interval (because the state variable must be continuous). For the slip law, it is convenient to set $\Theta = \exp\Psi$ and then Ψ is given by

$$\Psi(T) = \left(\Psi_1 + \ln V_2\right) \exp\left(-V_2\left(T - T_2\right)\right) - \ln V_2 \tag{12}$$

where, as with (11), Ψ_1 is the value at the end of the preceding interval.

Figure 1 plots results for steps in velocity at constant normal stress. Steady sliding at the reference velocity $V = 1$ occurs until $T = 2$. Velocity is suddenly increased to $V = 10$ at $T = 2$, then is decreased back to $V = 1$ at $T = 4$. The top panel shows

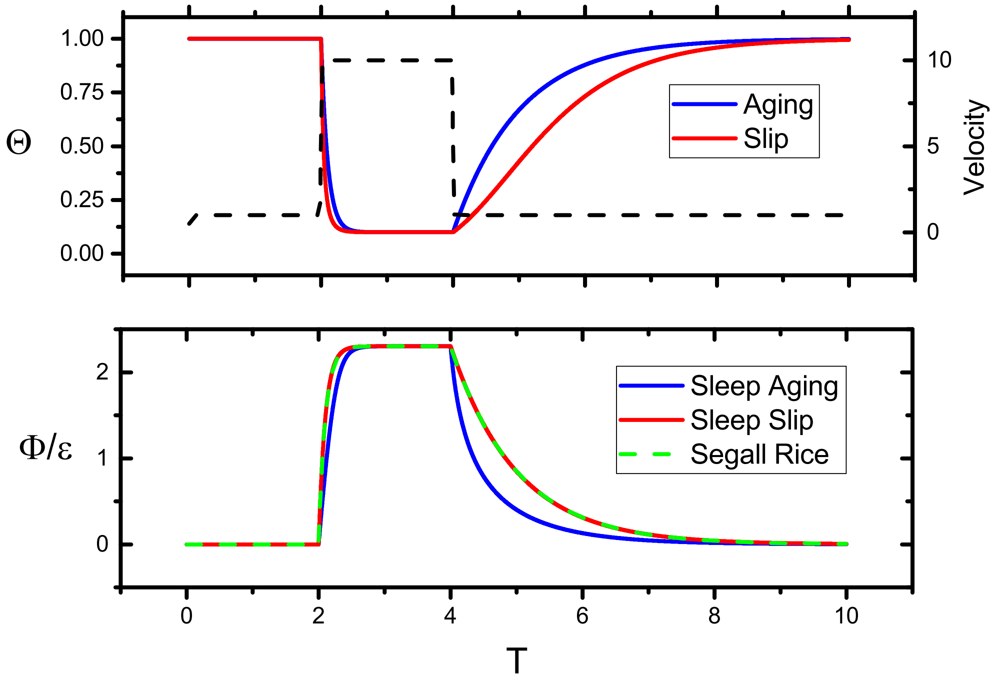

Figure 1. Results for imposed steps in sliding velocity at constant normal stress.

the variation of the state variable for the aging (2) and slip (3) laws. The dashed black line and right axis show the imposed velocity. The bottom panel shows the change in porosity Φ divided by ε for the SR and SL expressions for the slip and aging laws. The SR expression depends only on the velocity and, hence, is the same for the two state laws and, as noted above, is identical to the SL expression with the slip law. As shown, the predicted responses are similar.

Jumps in Effective Normal Stress at Constant Slip Velocity

Linker and Dieterich (1992) showed that for a jump in effective normal stress from $\bar{\sigma}_-$ to $\bar{\sigma}_+$ the state after the jump Θ_+ is described by

$$\Theta_+ = \Theta_- \left(\bar{\sigma}_-/\bar{\sigma}_+\right)^{\alpha/b} \tag{13}$$

where Θ_- is the value of the state before the jump. Because (8) does not depend on the state, the porosity calculated from the SR expression is not affected by the normal stress jumps (at constant slip velocity). Because the Linker and Dieterich (1992) term (5) is zero if the effective normal stress is constant, the term does not contribute in the intervals between the jumps. Consequently, equations (11) to (12) can be used taking account that the values of the state must be updated according to (13) at times when the jumps occur.

Figure 2 shows results for sliding at the reference velocity but with an effective normal stress increase of 5% at $T = 2$ and then a decrease of 5% (from the elevated value) at $T = 5$ for $\mu_0 = 0.6$, $b = 0.01$ and $\alpha = 0.2$. The top panel shows the change in state for the two state variable laws and the bottom the porosity divided by ε. The dashed black line in the top panel (and right axis) shows the variation of effective normal stress divided by $\bar{\sigma}_0$. Results are shown for both the aging (2) and slip (3) laws. Because the

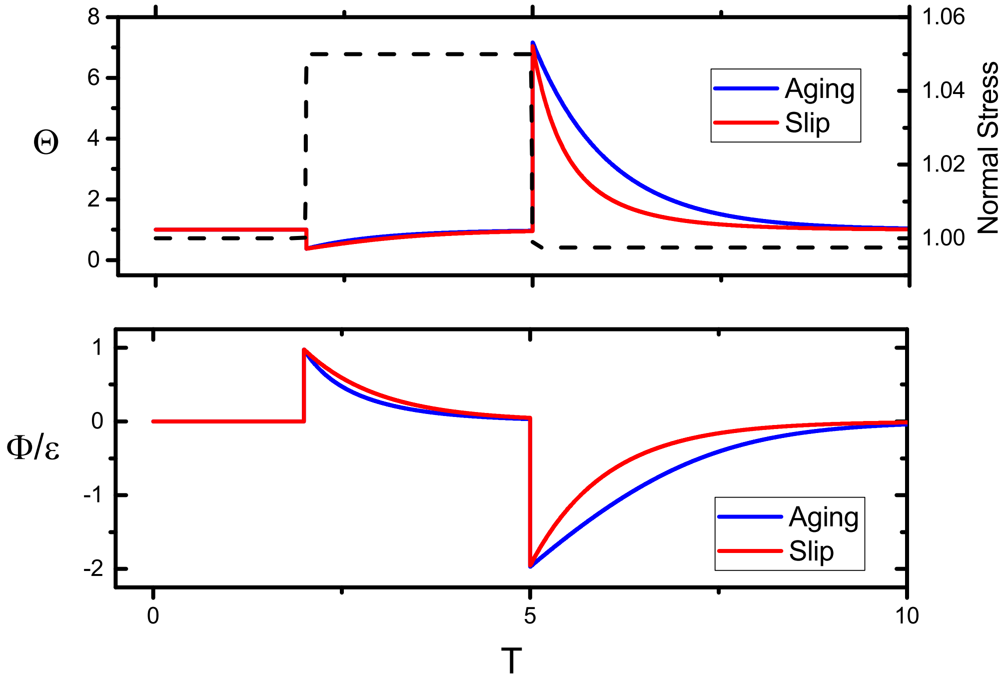

Figure 2. Results for sliding at the reference velocity $V = 1$ with normal stress jumps. $\mu_0 = 0.6$, $b = 0.01$

velocity is constant, the SR expression predicts that the porosity does not change. The difference between the results for the two state laws is small. The predicted change in the porosity is also small but significant compared to zero for the SR porosity expression.

Spring - Block Model

An example of a slide-hold-slide test and a simulation of the effects of the differences in the porosity formulations on slip events can be illustrated using the spring - block model of SR. A rigid block of unit area is loaded by a constant normal stress σ_0 and slides on a narrow layer with porosity ϕ and pore pressure p. The block is attached to a spring with stiffness k that is pulled at a constant speed v_0. The layer exchanges fluid with a remote reservoir at a distance L that is held at a constant pressure p_∞. The equation of motion for the block is given by

$$\dot{\tau} = k\left(v_0 - v\right) - \eta\dot{v} \tag{14}$$

where the superposed dot denotes the derivative with respect to time. The second term on the right employs the radiation damping approximation (Rice, 1993; Rice & Tse, 1986): the inertia, that is $m\dot{v}$, is replaced by ηv where $\eta = G/2v_s$. G is the shear modulus and v_s is the shear wave velocity. Flux of fluid mass to the layer is assumed to be proportional to the difference $p_\infty - p$ (Rudnicki & Chen, 1988). This assumption and fluid mass conservation lead to the following equation:

$$c^*\left(p_\infty - p\right) = \dot{p} + \phi/\beta \tag{15}$$

where c^* is the reciprocal of a time constant for fluid diffusion that can be expressed in terms of a diffusivity c as $c^* = c/L^2$. The compressibility β is equal to $\phi_0\left(\beta_f + \beta_\phi\right)$ where

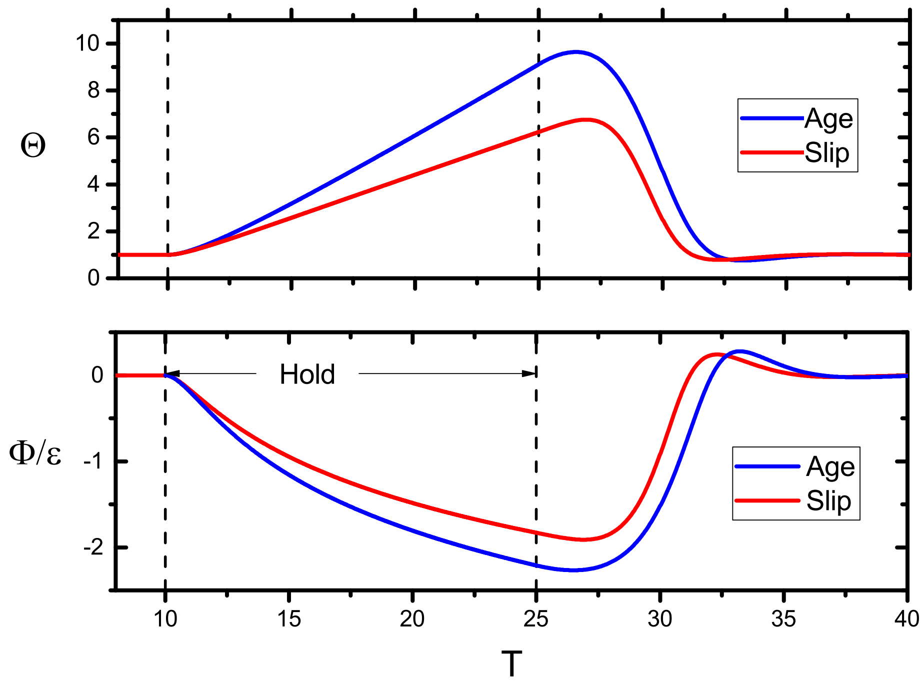

Figure 3. Variation of state (top) and porosity change (divided by ε) (bottom) with time for a simulation of a slide-hold-slide test. $\mu_0 = 0.6$, $a = 0.015$, $b = 0.01$, $kd_c/\sigma_0 = 0.01$, $\hat{\eta} = 10^{-6}$

β_f is the compressibility of the pore fluid and β_ϕ is the compressibility of the pore space. Although the spring-block model is too simple to describe slip in a continuum, it is a reasonable approximation for a laboratory experiment in which sliding occurs nearly simultaneously on the entire surface within the precision of the measurements. The variables can be nondimensionalized as above following (8) with, in addition, $C = c^* d_c/v_0$, $P = p/\sigma_0$, $\Sigma = \tau/\sigma_0$, $\hat{\eta} = \eta v_0/\sigma_0$ and $\hat{\beta} = \beta\sigma_0$ where σ_0 is the constant total normal stress.

When C is large, $p \approx p_\infty$ because fluid mass exchange between the remote reservoir and the porous layer occurs rapidly and conditions are said to be drained. In this case, Ruina (1983) showed that slip becomes unstable, in the sense that small perturbations from steady sliding grow exponentially in time, when the steady state response is velocity weakening ($b > a$, see (4)) and the spring stiffness k is less than a critical value given by

$$k_{crit} = (\sigma - p)\,(b - a)\,/d_c \tag{16}$$

Consequently, k is nondimensionalized by setting $K = k/k_{crit}$. When C is small, the fluid mass in the layer is constant and conditions are said to be undrained. SR have given an expression for the critical spring stiffness for undrained conditions and for the dependence of the critical value of k on C.

Differentiating (1), setting to (14), using (2) or (3) with (5), (8) or (9) and (15), leads to four first order ordinary differential equations for the velocity, state, porosity and pore pressure. The stress can be determined by using (14) as a fifth equation or by substitution into (1).

Slide-Hold-Slide

A slide-hold-slide test can be simulated by specializing the spring-block model just-described to drained conditions. In this case, the pore fluid pressure is constant and can be taken as zero. Equation (15) is not needed. The same normalizations apply with the one exception that the spring stiffness k is made nondimensional by dividing by σ_0/d_c (omitting the factor $b-a$). The value of kd_c/σ_0 is arbitrarily taken to be 0.01. The simulation begins with steady sliding at the reference velocity $V = 1$. At $T = 10$, the load point velocity v_0 is set equal to zero for $\Delta T = 15$ (For the values $v_0 = 10\mu$m/s and $d_c = 0.2$ mm, cited earlier as representative of laboratory experiments, this corresponds to 300 seconds.) Then pulling at the reference velocity is resumed.

Figure 3 shows the variation of the state and the porosity according to the SR and SL formulations as a function of time. The porosity change for SR does not depend on the state and, as shown earlier, is identical to the SL expression with the slip law. The predictions of the SR and SL formulations differ, though not dramatically. Both predict a decrease in porosity during the hold time as observed by Karner and Marone (2001). Limited exploration indicated that the maximum shear and porosity after resliding were linear with the logarithm of hold time, consistent with experimental observations (Karner & Marone, 2001).

Effects of Pore Pressure Changes on Slip Velocity

This section presents an example of the difference in the response of the spring - block system for the SR (8) and SL (9) expressions for the variation of porosity. Calculations use the aging law. The principal parameters controlling the response are the nondimensional diffusivity C and the nondimensional stiffness K. Results are given for $K = 0.25$ and $C = 1$. Other parameters are $\varepsilon = 1.7 \times 10^{-4}$, $\hat{\beta} = 7 \times 10^{-3}$, $\mu_0 = 0.64$, $a = 0.010$, $b = 0.015$, $\hat{\eta} = 10^{-12}$, $\alpha = 0.3$ and $P_\infty = 0.2$. Initial conditions are $V = 1.05$, $\Theta = 1/1.05$, $\Phi = 0$, $P = 0.2$, and $\Sigma = (1 - 0.2)\,\mu_0$. For values of C larger than about 10 conditions approach drained. In this case the response for the two variations in porosity variation is small because changes in the effective normal stress due to pore pressure changes are small. For values less than 0.1, the response is close to undrained and the response is strongly damped because of dilatant hardening (Segall & Rice, 1995).

Figure 4 shows the logarithm of $V = v/v_0$, and the change in porosity $\Phi = \phi - \phi_0$, divided by ε, against the nondimensional time $T = v_0 t/d_c$. In the first column, the results for SL and SR can barely be distinguished for the velocity (first row) and pore pressure (last row). The porosity change (middle) also appears to differ little near the rapid slip events (peaks). Between the peaks, when the slip velocity is slow, there is a clear difference between SR and SL. Porosity decreases are much larger for SL. Presumably, this occurs because SL depends on the state and for the aging law the state is still changing even when the slip velocity is low. This difference does not, however, appear to have much effect on the pore pressure.

The second column of Figure 4 gives an expanded view near the peak at $T = 1387$ for SR and $T = 1404$ for SL. Although the interval between the peaks is barely distinguishable at the scale of the left column, it corresponds to about 5.67 minutes for the values of d_c and v_0 (0.2 mm and 10μm/s) representative for the laboratory and 5.67 years for crustal scale values (0.01 m and 0.03 m/year). The shapes of the velocity peaks are similar and despite the difference in the porosity variations between the slip peaks, their variation near the peaks is similar. The shapes of the pore pressure changes at the peaks appear to be identical, just offset, but overlaying them does show some differences.

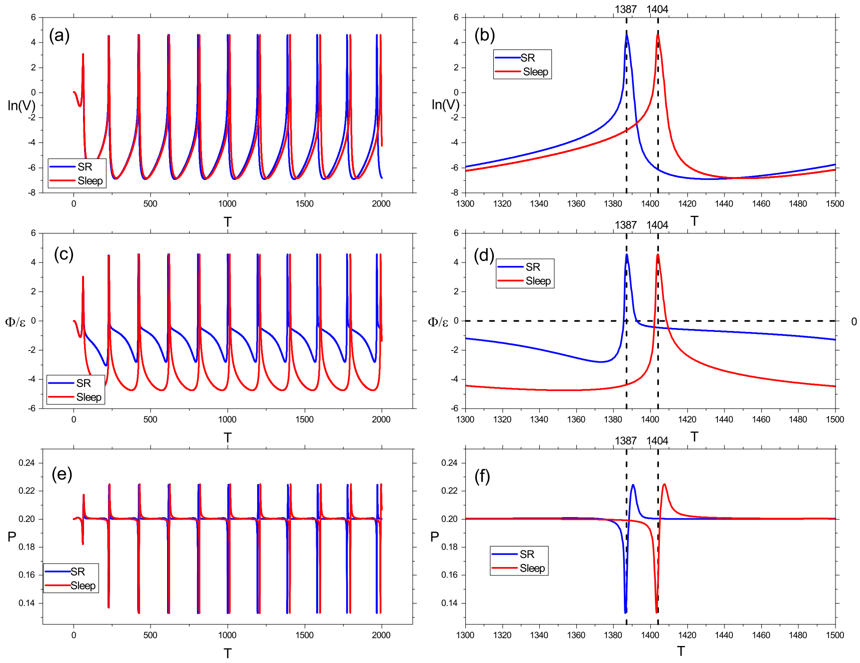

Figure 4. The first column shows plots of the logarithm of the nondimensional velocity (a), the porosity change, divided by ε (c), and the nondimensional pore pressure (e) against nondimensional time for the SR (blue) and SL (red) porosity formulations. The second column shows the same quantities on an expanded time scale near one of the rapid slip events.

Discussion

The results of using the SR and SL expressions for the porosity evolution are similar. Both have the same steady state and both fit the data of Marone et al. (1990) equally well (SR). Samuelson et al. (2009) use SL to fit their data but they do not remark whether SR also fits their data. As pointed out earlier, for the slip law the porosity predictions of SR and and SL are identical. In addition, the two porosity formulations do not differ dramatically for the simulations of a velocity stepping and a slide-hold-slide test. Nevertheless, there are differences. The principal one is that because the SR law depends only on the slip velocity the porosity does not change for effective normal stress changes at constant sliding velocity (assuming ε is constant). The effective normal stress is changed by changes in pore pressure and pore pressure changes are linked to porosity variations (by (15)) for the spring-block model). Consequently, even in the simple spring-block model, there can be a complex interplay between the porosity and the pore pressure. At first glance for the spring block simulation (first column of Figure 4), the effect does not appear to be large except for the porosity variation in the interval of slow slip between rapid slip events. Closer examination (second column of Figure 4) indicates that the difference in time between the peaks is significant.

There are caveats. Only a few simulations are presented here. Although these are likely representative, testing a much wider range of parameters might reveal modified results. Also, the simulations here are for the spring-block model rather than slip in a continuum. More importantly, it is fair to say that the formulations are based on a limited amount of data (Marone et al., 1990; Samuelson et al., 2009). The subject seems sufficiently important that further experimental investigation is warranted. For example, based on their experiments, Proctor et al. (2020) argue that the effects of pore fluid change can exceed those due to rate and state effects. Another issue is the dependence of ε on the effective normal stress. Although the experiments of Samuelson et al. (2009) find that it does not, the possible dependence of ε on effective stress, and perhaps, on the state of the surface or gouge layer is in need of further exploration.

Proctor et al. (2020) used a miniature pore pressure sensor placed near a saw cut to directly measure pore pressure changes near a slipping fault in Westerly granite. They examine two configurations: one is a bare rock slip surface; the other is a 2 mm wide quartz gouge layer between granite blocks. They observe one rapid slip event on the bare rock surface followed by three slow events and four slow events on the fault with gouge. Their observations for the rapid slip event can be compared with the calculations shown in Figure 4. Their Figure 2c shows a slow increase in pore fluid pressure preceding the slip event which they surmise is due to compaction. Figure 4d here does show compaction preceding the slip event but essentially no change in pore pressure. Although the permeability is small (10^{-20} m^2) the relevant comparison is the time scale of compaction with that of fluid diffusion. Because the latter is fast compared with the former in the simulation, flow from the reservoir maintains the pore pressure. Proctor et al. (2020) remark that the compaction preceding the rapid slip event is "inconsistent with standard brittle and frictional models of failure (Brace, 1963; Segall & Rice, 1995) that involve precursory dilation" but that is not the case with the simulation here. Consistent with their observations, this slow compaction is followed by rapid dilation with corresponding pressure decrease coincident with the slip event. Immediately after the slip event the pore pressure increases and reaches a maximum. Proctor et al. (2020) suggest that this increase could be due to compaction associated with afterslip or local fluid flow. The simulation suggests the former (although because the fluid mass flux is assumed to be proportional to the difference in pore pressure in the reservoir and on the the fault, there is no local fluid flow). For the values of v_0 and d_c cited earlier as representative of experiments, the maximum occurs about 20 s after the rapid slip event which, from their Figure 2c, appears to be similar to that in the experiment. However, Proctor et al. (2020) report that the premonitory compaction reverses within 1 s of rupture but the time difference in the simulation is much longer.

The measurements of Proctor et al. (2020) show that changes in pore pressure cause a greater change in the shear stress than that due to the changes due to rate and state friction. Although not shown here, this is also the case in the spring-block simulation. The pore pressure changes are about an order of magnitude larger than the changes in the effective friction coefficient. This difference is about the same as Proctor et al. (2020) observe for their slow events, but much larger than they observe for the rapid slip event. Despite the larger dilation in the simulation, it is not sufficient to stabilize the rapid slip event. This is likely due to the small value of K and the not sufficiently small value of C chosen for this simulation. Nevertheless, the pore pressure does have a significant effect on the response (as demonstrated by SR). If the same simulation is done with no pressure change, the frequency and magnitude of the slip events are quite different.

Despite the qualitative agreement of the simulations with the observations, with the exception of constant pore fluid pressure during compaction prior to the rapid slip event, and some quantitative agreement, it is difficult to make more detailed quantitative comparisons for several reasons. One is that the experiment was conducted in axisymmetric compression for which the total normal stress on the slip surface is coupled to the shear stress and, hence, not constant. In the simulation, the total normal stress is constant. Another is that the values of the nondimensional spring stiffness K and diffusion C are chosen arbitrarily. Also, fluid diffusion is approximated by assuming that the fluid mass flux is proportional to the difference between the pore pressure on the slip surface and in the reservoir. A more realistic formulation would use Darcy's law for which the mass flux is proportional to the gradient of the pore fluid pressure. Nevertheless, the results of the simulation are consistent with the observations of Proctor et al. (2020) near the rapid slip event. Of course, a big difference is the repeated roughly periodic occurrence of rapid slip events in the simulations and the observed more frequent occurrence of slow slip events in the experiment.

Conclusion

This paper has compared the porosity relations suggested by SR and by SL. They are investigated here using simulations of velocity stepping, slide-hold-slide and normal effective stress jump experiments and of the response of a spring-block model. Although there are many similarities between the predictions of the two laws, there are differences that can be important. In particular, only in the SL formulation do normal effective stress changes cause a porosity change at constant slip velocity. In addition, a simulation with the spring-block model indicates that the predicted time between rapid slip events for the two formulations is significant. This difference could be important in applications in which the effective normal stress is altered by changes in pore pressure. These include processes involving fluid injection or withdrawal and pore pressure changes induced by fault propagation and slip. In addition, the results of the spring-block simulation are, with one exception, qualitatively consistent with the observations of Proctor et al. (2020) near a rapid slip event. An issue not investigated here is the possible dependence of the magnitude of the effects (ε, in both formulations). The two formulations are based on limited experimental data and the calculations here suggest that the issue of an appropriate representation of porosity changes is in need of further experimental and theoretical work.

Open Research

This is a theoretical paper and contains no new data.

Acknowledgments

I am grateful for financial support from the National Science Foundation Geophysics Program through award number EAR-2120374.

References

Ake, J. K., O'Connell, D., & Block, L. (2005). Deep-injection and closely monitored induced seismicity at Paradox Valley, Colorado. *Bulletin of the Seismological Society of America*, *95*, 664-683. doi: 10.1785/0120040072

Ampuero, J.-P., & Rubin, A. M. (2008). Earthquake nucleation on rate and state faults–aging and slip laws. *Journal of Geophysical Research: Solid Earth*, *113*(B1).

Barbour, A. J., Norbeck, J. H., & Rubinstein, J. L. (2017). The effects of varying injection rates in Osage County, Oklahoma, on the 2016 Mw 5.8 Pawnee earthquake. *Seismological Research Letters*, *140-153*(Art. 4), 38.

Bhattacharya, P., Rubin, A. M., Tullis, T. E., Beeler, N. M., & Okazaki, K. (2022). The evolution of rock friction is more sensitive to slip than elapsed time, even at near-zero slip rates. *Proceedings of the National Academy of Sciences*, *119*(30), e2119462119.

Brace, W. (1963). Brittle failure of rocks. In W. R. Judd (Ed.), (p. 110-178). Elsevier.

Byerlee, J. (1978). Friction of rocks. *Pure and Applied Geophysics*, *116*(4-5), 615-626.

Charéty, J., Cuenot, N., Dorbath, L., Dorbath, C., Haessler, H., & Frogneux, M. (2007). Large earthquakes during hydraulic stimulations at the geothermal site of Soultz-sous-Forêts. *International Journal of Rock Mechanics and Mining Sciences*, *44*, 1091-1105.

Deichmann, N., & Giardini, D. (2009). Earthquakes induced by the stimulation of an enhanced geothermal system below Basel (Switzerland). *Seismological Research Letters*, *80*(5), 784-798. doi: doi:10:1789/gssrl.80.5.784

Dieterich, J. H. (1979). Modeling of rock friction: 1. experimental results and constitutive equations. *Journal of Geophysical Research: Solid Earth*, *84*(B5), 2161–2168.

Dieterich, J. H. (1980). Experimental and model study of fault constitutive properties. *Solid Earth Geophysics and Geotechnology*, *42*, 21–29.

Ellsworth, W. L. (2013). Injection-induced earthquakes. *Science*, *341*. doi: 10.1126/science.1225942

Evans, K. F., Zappone, A., Kraft, T., Deichmann, N., & Moia, F. (2012). A survey of the induced seismic responses to fluid injection in geothermal and CO_2 reservoirs in Europe. *Geothermics*, *41*, 30-54.

Healy, J. H., Rubey, W. W., Griggs, D. T., & Raleigh, C. B. (1968). The Denver earthquakes. *Science*, *161*, 1301 - 1310.

Heimisson, E. R., Rudnicki, J., & Lapusta, N. (2021). Dilatancy and compaction of a rate-and-state fault in a poroelastic medium: Linearized stability analysis. *Journal of Geophysical Research: Solid Earth*, *126*(8), e2021JB022071.

Hong, T., & Marone, C. (2005). Effects of normal stress perturbations on the frictional properties of simulated faults. *Geochemistry, Geophysics, Geosystems*, *6*(3).

Horton, S. (2012). Disposal of hydrofracking waste fluid by injection into subsurface aquifers triggers earthquake swarm in central Arkansas with potential for damaging earthquake. *Seismological Research Letters*, *83*(2), 250-260. doi: 10.1785/gssrl.83.2.250

Hsieh, P. A., & Bredehoeft, J. D. (1981). A reservoir analysis of the Denver earthquakes. *Journal of Geophysical Research*, *86*(B2), 903 - 920.

Karner, S. L., & Marone, C. (2001). Fractional restrengthening in simulated fault gouge: Effect of shear load perturbations. *Journal of Geophysical Research: Solid Earth*, *106*(B9), 19319–19337.

Keranen, K. M., Savage, H. M., Abers, G. A., & Cochran, E. S. (2013). Potentially induced earthquakes in Oklahoma, USA: Links between wastewater injection and the 2011 Mw 5.7 earthquake sequence. *Geology*, *41*(6), 699-702. doi: 10.1130G34045.1

Keranen, K. M., Weingarten, M., Abers, G. A., Bekins, B. A., & Ge, S. (2014). Sharp increase in central Oklahoma seismicity since 2008 induced by massive wastewater injection. *Science*, *345*(6195), 448-451. doi: 10.1126/science.1255802

Kim, W.-Y. (2013). Induced seismicity associated with fluid injection into a deep well in Youngstown, Ohio. *Journal of Geophysical Research*, *118*, 3506-3518. doi: 10.1002/jgrb.50247

Lapusta, N., & Barbot, S. (2012). Models of earthquakes and aseismic slip based on laboratory-derived rate and state friction laws, vol. 661. *Research Signpost, Kerala, India*, *840*.

Lapusta, N., Rice, J. R., Ben-Zion, Y., & Zheng, G. (2000). Elastodynamic analysis for slow tectonic loading with spontaneous rupture episodes on faults with rate- and state-dependent friction. *Journal of Geophysical Research*, *105*, 23,765 - 23,789.

Lengliné, O., Boubacar, M., & Schmittbuhl, J. (2017). Seismicity related to the hydraulic stimulation of GRT1, Rittershoffen, France. *Geophysical Journal International*, *208*(3), 1704–1715.

Linker, M. F., & Dieterich, J. H. (1992). Effects of variable normal stress on rock friction: observations and constitutive equations. *Journal of Geophysical Research*, *97*, 4923-4940.

Liu, Y., & Rice, J. R. (2005). Aseismic slip transients emerge spontaneously in three-dimensional rate and state modeling of subduction earthquake sequences. *Journal of Geophysical Research: Solid Earth*, *110*(B8).

Majer, E. L., Baria, R., Stark, M., Oates, S., Bommer, J., Smith, W., & Asanuma, H. (2007). Induced seismicity associated with enhanced geothermal systems. *Geothermics*, *36*, 185-222.

Marone, C. (1998). Laboratory-derived friction laws and their application to seismic faulting. *Annual Review of Earth and Planetary Sciences*, *26*(1), 643–696.

Marone, C., Raleigh, C. B., & Scholz, C. H. (1990). Frictional behavior and constitutive modeling modeling of simulated fault gouge. *Journal of Geophysical Research*, *95*, 7007 - 7025.

Martinez-Garzón, P., Kwiatek, G., Sone, H., Bohnhoff, M., Dresen, G., & Hartline, C. (2014). Spatiotemporal changes, faulting regimes, and source parameters of induced seismicity: A case study from the Geysers geothermal field. *Journal of Geophysical Research*, *120*, 8378-8396. doi: 10.1002/2014JB011385

Perfettini, H., Schmittbuhl, J., Rice, J. R., & Cocco, M. (2001). Frictional response induced by time-dependent fluctuations of the normal loading. *Journal of Geophysical Research: Solid Earth*, *106*(B7), 13455–13472.

Proctor, B., Lockner, D., Kilgore, B., Mitchell, T., & Beeler, N. (2020). Direct evidence for fluid pressure, dilatancy, and compaction affecting slip in isolated faults. *Geophysical Research Letters*, *47*(16), e2019GL086767.

Raleigh, C. B., Healy, J. H., & Bredehoeft, J. D. (1976). An experiment in earthquake control at Rangely, Colorado. *Science*, *91*, 1230 - 1237.

Rice, J. R. (1993). Spatio-temporal complexity of slip on a fault. *Journal of Geophysical Research*, *98*(B6), 9885-9907.

Rice, J. R., & Tse, S. T. (1986). Dynamic motion of a single degree of freedom system following a rate and state dependent friction law. *Journal of Geophysical Research*, *91*(B1), 521-530.

Rudnicki, J. W., & Chen, C.-H. (1988). Stabilization of rapid frictional slip on a weakening fault by dilatant hardening. *Journal of Geophysical Research: Solid Earth*, *93*(B5), 4745–4757.

Ruina, A. (1983). Slip instability and state variable friction laws. *Journal of Geophysical Research: Solid Earth*, *88*(B12), 10359–10370.

Samuelson, J., Elsworth, D., & Marone, C. (2009). Shear-induced dilatancy of fluid-saturated faults: Experiment and theory. *Journal of Geophysical Research: Solid Earth*, *114*(B12).

Segall, P., Grasso, J.-R., & Mossop, A. (1994). Poroelastic stressing and induced seismicity near the Lacq gas field, southwestern France. *Journal of Geophysical Research: Solid Earth*, *99*(B8), 15423–15438.

Segall, P., & Rice, J. R. (1995). Dilatancy, compaction, and slip instability of a fluid-inflitrated fault. *Journal of Geophysical Research*, *100*(B11), 22155-22171.

Segall, P., Rubin, A. M., Bradley, A. M., & Rice, J. R. (2010). Dilatant strengthening as a mechanism for slow slip events. *Journal of Geophysical Research*, *115*(B12305). doi: 10.1029/2010jb007449

Sleep, N. H. (1995). Ductile creep, compaction, and rate and state dependent friction within major fault zones. *Journal of Geophysical Research: Solid Earth*, *100*(B7), 13065–13080.

Weingarten, M., Ge, S., Godt, J. W., Bekins, B. A., & Rubinstein, J. L. (2015). High-rate injection is associated with the increase in U.S. mid-continent seismicity. *Science*, *348*(6241), 1336-1340.

Yang, Y., & Dunham, E. M. (2021). Effect of porosity and permeability evolution on injection-induced aseismic slip. *Journal of Geophysical Research: Solid Earth*, *126*(7), e2020JB021258.

Zoback, M. D., & Harjes, H.-P. (1997). Injection-induced earthquakes and crustal stress at 9 km depth at the KTB deep drilling site, Germany. *Journal of Geophysical Research*, *102*(B8), 18,477-18,491.